FORMATION OF $Y_x Nd_{1-x} Ba_2 Cu_3 O_{7-\delta}$ (0 ≤ x ≤ 0.7) SUPERCONDUCTORS FROM AN UNDERCOOLED MELT VIA AERO-ACOUSTIC LEVITATION

D.E. Gustafson, W.H. Hofmeister, and R.J. Bayuzick

Materials Science and Engineering, Vanderbilt University

INTRODUCTION

Melt processing of RE123 superconductors has gained importance in recent years. While the first high temperature superconductors (HTSCs) were made using traditional ceramic press and sinter technology, recent fabrication efforts have employed alternate processing techniques including laser ablation and ion beam assisted deposition for thin film fabrication of tapes and wires and melt growth for bulk materials.[1-4] To optimize these techniques and identify other potential processing strategies, phase relation studies on HTSCs have been conducted on a wide variety of superconducting compounds using numerous processing strategies. This data has enhanced the understanding of these complex systems and allowed more accurate modeling of phase interactions. All of this research has proved useful in identifying processing capabilities for HTSCs but has failed to achieve a breakthrough for wide spread application of these materials. To overcome drawbacks of the sintered material, many researchers have developed new processing routes involving melt processing techniques. Melt processing has significantly advanced the state-of-the-art understanding of superconductivity in polycrystalline bulk materials and has produced materials with J_c of greater than 10^4 A/cm^2.[5] The melt processed materials produced, however, suffer from several shortcomings. Due to incongruent melting of RE123 at high temperatures, liquid phase flows out of the interior of the material resulting in voids, and Ba-Cu rich liquid inclusions may become trapped between grains reducing superconductive properties. Processing rates are very slow, *i.e.* on the order of 50 mm/h for a 25 mm^2 cross sectional area sample.[6] Slow processing rates can also expose the material to moisture and CO_2 which are highly reactive with copper oxide superconductors.[7] Also, distortions and macrocracks form due to severe shrinkage accompanying the melt processing. Large complex shapes are therefore difficult to fabricate by melt processing and the only shapes reported to date have been either disks or bars.[8]

Several researchers have examined the effect of mixed rare earth (RE) atoms in the 123 system referred to as RE123 alloys. Work to date has included oxygen-controlled-melt-growth of RE123 alloys, containerless drop tube processing of RE123 alloys, and directional solidification of RE123 alloys.[9-14] Interesting results include a higher crystallization rate for the alloy compared to the single RE system and a sharper critical temperature (T_c) as well as a higher critical current (J_c) in the alloy compared to the single RE system. Additionally, the liquidus for $Y_{.1-x}Nd_x Ba_2 Cu_3 O_{7-\delta}$ was measured by J. R. Olive by processing in a drop tube, and a minimum in the liquidus was found for composition $Y_{.1}Nd_{.9}Ba_2 Cu_3 O_{7-\delta}$ at 1500°C (±25°C).[15] Additional studies of mixed alloy systems may reveal thermodynamic and kinetic parameters favorable for the fabrication of HTSCs with superior properties.

This study examines the role of full to partial substitution of Nd in the Y123 structure under rapid solidification conditions. Aero-acoustic levitation (AAL) was used to levitate and undercool RE123 in pure oxygen binary alloys with RE = Nd and Y along a range of compositions corresponding to $Y_xNd_{1-x}Ba_2Cu_3O_{7-\delta}$ ($0 \leq x \leq 0.7$) which were melted by a CO_2 laser. Higher Y content spheres could not be melted in the AAL and were excluded from this report. Solidification structures were examined using scanning electron microscopy, electron dispersive spectroscopy, and powder x-ray diffraction to characterize microstructures and identify phases.

I. Experimental Method

Starting powders of orthorhombic RE123 were supplied by Superconductive Components, Inc., fabricated using standard ceramic press and sinter techniques. Levitation spheres were then fabricated in a copper hearth under flowing O_2. The aero-acoustic levitator (AAL) consisted of a O_2 gas jet coupled with a three-axis acoustic positioning system for levitation of samples.[16] The O_2 gas jet was pre-heated to approximately 400°C in the AAL. Melting of samples was accomplished using a CO_2 laser powered by a Rofin-Sinar 1700 SM power supply. The laser beam was split and focused onto opposing sides of each specimen, perpendicular to the gas jet flow. Samples were 2 mm diameter spheres having a mass of 30-50 mg. A typical experiment involved levitating the sample in the O_2 gas jet and heating it with the laser until liquid vortex currents were visible on the surface. After several seconds, the laser beam was shut off and the sample allowed to radiantly cool at 300-400°C/s. Temperature measurements were made using a two-color pyrometer with Si and InGaAs detectors, and recalescence events were recorded using a Kodak EKTAPRO HS Motion Analyzer Model 4540 operating at 4500 frames/s. The resulting samples were examined using scanning electron microscopy, energy dispersive spectroscopy, and powder x-ray diffraction to identify phases and characterize microstructures.

II. Results

Samples were melted by the laser while being levitated and were undercooled several hundred degrees relative to the liquidus before solidification. Solidification of the samples was accompanied by a distinct recalescence event which lasted between 0.2 and 0.3 seconds where the increased emissive intensity was visible to the naked eye. Solidification events varied considerably in duration and intensity depending upon the composition of the sample, but the general solidification mechanism appears to be similar. After the laser was blocked and the sample cooled a few seconds, swirling particles roughly 100 μm in size were seen on the surface of the melt as it spun while levitated. These particles increased in number as the undercooling increased. Solidification events recorded by the Kodak EKTAPRO camera confirmed these observations. Eddies in the swirling melt were observed drawing the particles to a preferred location near the top of the sphere. As the sample continued to cool, the particles continued to cluster until a solid front was seen growing from the top to the bottom of the sphere surface. This front wrapped around the surface of the sphere, enveloping the melt with a shell of solid material. The recalescence event occurred simultaneously and was marked by a distinct flash of light. In this study, the as-solidified morphology of samples fully melted in the AAL can be generalized into three zones, and the zones appear to be caused by thermal gradients across the samples during processing. The first zone encompasses the outer layer of the sphere which solidified first. Here, solidification of the melt proceeded quickly. This outer zone is composed of relatively void-free RE123 and the morphology can be described as faceted. The formation of this layer involved the release of latent heat and resulted in a recalescence event which was recorded by the pyrometer and EKTAPRO camera. The thickness of

this outer layer appears to be a function of composition and varied from a maximum of 500 μm for the Nd rich samples to 200 μm and less for the Y rich samples. In this region, the sample was undercooled, and RE123 formed directly from the undercooled melt. The second zone which lies between the outer zone and the center of the sphere is a relatively thin transitional region where RE211 dendrites are surrounded by RE123 dendrites. The temperature gradient in the sphere just prior to recalescence caused this region to be heated above the peritectic transformation temperature (T_p), and there was no undercooling relative to T_p. The local conditions for the second zone are also altered by formation of the outer zone which further slowed the cooling rate of the bulk of the sphere. The RE211 dendrites in this region solidified heterogeneously at the interface of the solid RE123 and the melt. The dendrites are fine but coarsen closer to the center of the sphere. The third zone is located near the center of the sphere generally adjacent to the shrinkage voids and is dominated by coarse RE211 dendrites with interdendritic Ba-Cu-O. This final zone was formed as the sphere continued to cool, and the microstructure indicates solidification of the zone without undercooling. The Ba-Cu-O liquid, cooled sufficiently and unable to react quickly with the RE211 to form RE123, solidified around the RE211 dendrites.

III. Discussion

Containerless processing with aero-acoustic levitation allows for cooling of molten ceramic samples several hundred degrees below the liquidus until spontaneous crystallization or recalescence occurs. Cooling curves for the processed samples reveal characteristic events which correspond to the release of the latent heat of fusion and the peritectic decomposition temperature (T_p) for RE123. In this work, the uncorrected recalescence temperatures for Nd123 was indicated to be 1043°C (±17°C), and the maximum recalescence temperature was assumed to correspond to T_p for each composition. This indicated temperature is below the previously reported value of T_p for Nd123 by 66°C. Prado et al. report the T_p to be 1109°C for Nd123 in pure oxygen.[17] Kambara et al. report the T_p for Nd123 in oxygen to be 1112°C.[18] The absolute differences between the reported values and the experiments detailed in this report are attributed to error in the pyrometer which was used to measure temperature in the experiments reported here. This disagreement could not be experimentally confirmed because the pyrometer failed prior to independent calibration. However, by using the difference between the experimental and reported values for Nd123 as an in-situ calibration factor, the experimental data was corrected to reflect the actual transformation temperatures for the compositions studied in this work.

Figure 1 is a compilation of the average recalescence events for the binary alloys composed of Nd-Y. For purposes of illustration the traces in Figure 1 are synchronized at the moment of recalescence. The curves were determined by ignoring the erratic events recorded and averaging the temperature as a function of time to represent the characteristic event for each composition. Also, the in-situ calibration factor has been applied to the curves to reflect the transformation temperatures. There appears to be some correlation between the size of the recalescence event, as given by the area under the time versus temperature plot, and the volume fraction of RE123 formed from the melt as shown by microstructural examination. The area fraction of RE123 in the micrographs or the volume fraction in the bulk and the size of the recalescence event decreases with increasing Y content of the alloy, or, equivalently, the fraction of RE211 increases with increasing Y content. Although the differences between alloys with less than 50% Y are less pronounced, increasing Y content above 50% dramatically increases the fraction of RE211 which forms during processing in the AAL. The binary alloy compositions rich in Nd revealed the most distinct recalescence events and were the most successful for obtaining relatively single phase RE123 during AAL processing.

Figure 2 is a plot of the experimental peritectic temperatures obtained in this report with error bars representing one standard deviation. These results are also plotted with the liquidus for the Nd-Y alloys for illustration in Figure 3.[19] This plot contains relevant data for researchers employing melt processing techniques. The minimum in the liquidus corresponds to a composition of Nd_9Y_1123 while the minimum in the peritectic corresponds to Nd_7Y_3123. The minimum in undercooling relative to the liquidus observed in these experiments, however, corresponds to 520°C (corrected) for samples with composition Nd_8Y_2123 and Nd_9Y_1123. Thus the range of compositions which undercooled less than 600°C to form RE123 directly from the melt extends from $Nd123$ to Nd_7Y_3123. The degree of undercooling for $Nd123$ to Nd_7Y_3123 samples corresponds to approximately 35% of the liquidus. Compositions more rich in Y undercooled more than 650°C below the liquidus to form RE123 directly from the melt, but a considerably larger volume fraction of RE211 appears in these specimens than in Nd rich specimens. The degree of undercooling for the Y-rich specimens was over 40% of the liquidus indicating that it is more difficult to form RE123 from the melt for Y-rich compositions.

Microstructural and pyrometry evidence seem to indicate that the volume fraction of RE123 formed directly from the melt increased as the Nd content in the Nd-Y composition increased. The compositional dependence of phase selection is also evident from a comparison of x-ray diffraction (XRD) spectra. Figure 4 is a comparative plot of XRD data for several Nd-Y alloys. Clearly evident in this plot is the large volume fraction of RE123 for all samples. Also prevalent is the appearance of RE211 peaks in the Y rich alloys. It is possible that the poor thermal conductivity and large degree of undercooling required combine to create large thermal gradients in the Y-rich samples. Thus, processing in the AAL resulted in only an outer shell of the sample which actually undercooled and formed RE123 directly from the melt. The phase stability of RE211 may also play a role in this outcome since RE211 is not a stable phase in the Nd123 system. Increasing the Y content may create favorable conditions for the formation of RE211 during rapid solidification processing in the AAL. The Nd rich binary alloys also have no appreciable second phases or byproducts indicating that the formation of RE123 is favored in the rapid solidification of a melt with a Nd-rich RE123 starting composition. Peaks corresponding to Pt which was present in the x-ray diffractometer are found in all XRD spectra in this report.

Previous processing studies of RE123 at near equilibrium conditions in high oxygen environments resulted in the partial substitution of RE^{3+} for Ba^{2+} and the formation of compounds with the formula $RE_{1+x}Ba_{2-x}Cu_3O_{7-\delta}$. This solid solubility behavior was determined to be undesirable since the RE123 solid solutions have inferior superconducting properties compared to the stoichiometric compounds.[20] Low oxygen partial pressure environments were used to avoid solid solution formation in near compensated by the addition of extra oxygen. Simply removing the oxygen removed the equilibrium melt processing because the substitution of RE^{3+} for Ba^{2+} must be opportunity for solid solution formation in those near-equilibrium processing techniques. In this study, no evidence of substitution of Nd^{3+} for Ba^{2+} was discovered even while processing the samples in pure oxygen. Thus it appears possible to solidify RE123 directly from the melt while effectively bypassing the formation of solid solutions using rapid solidification techniques in high oxygen partial pressure atmospheres.

IV. Conclusions

Aero-acoustic levitation is a very successful technique for melting, undercooling, and rapidly solidifying high temperature ceramic oxide superconductors. In this study, binary Nd/Y RE123 samples were melted, undercooled hundreds of degrees relative to the liquidus, and solidified to from RE123. Mixtures of Y123 and Nd123 result in a minimum for the peritectic temperature at

Nd_7Y_3123, 66°C below the peritectic of pure Nd123. Increasing Nd content in Nd/Y alloys results in the formation of a higher volume fraction of RE123. Nd-Ba solid solution behavior of the type $Nd_{1+x}Ba_{2-x}Cu_3O_{7-\delta}$ was not observed. The RE ratio in RE123 and RE211 structures formed during AAL processing mirrors the nominal starting composition of the bulk. Solidification structures are varied and complex but the processed sphere morphology can be summarized into three zones: relatively void-free RE123 at the surface, RE123 and RE211 transition, and RE211 with interdendritic Ba-Cu-O. Measurable changes occur in the RE211 lattice parameters because of Nd substitution for Y in the Y211 unit cell.

V. Acknowledgments

REFERENCES

1. J.R. Hull, JOM 51, 7, 12 (1999).
2. Goyal, R. Feenstra, F.A. List, M. Paranthanman, D.F. Lee, D.M. Kroeger, D.B. Beach, J.S. Morrell, T.G. Chirayil, D.T. Verebelyi, X. Cui, E.D. Specht, D.K. Christen, and P.M. Martin, JOM 51, 7, 12 (1999).
3. S. Foltyn, P. Tiwari, R. Dye, M. Le, and X. Wu, Appl. Phys. Lett. 63 1848-50 (1993).
4. Y. Iijima, N. Tanabe, O. Kohno, and Y. Ikeno, Appl. Phys. Lett. 60 769-771 (1992).
5. S. Jin, T.H. Tiefel, R.C. Sherwood, M.E. Davis, R.B. van Dover, G.W. Kammlott, R.A. Fastnacht, and H.D. Keith, Appl. Phys. Lett. 52 2074 (1988).
6. K. Salama A.S. Parikh, and L. Woolf, Appl. Phys. Lett. 68 14, 1993-1995 (1996).
7. M. Murakami, Appl. Supercond. 6, 2-5, 51-59 (1998).
8. E.S. Reddy, T. Rajasckharan, G.R. Kumar, T.V. Chandrasekhar Rao, V.C. Sahni, Mater. Sci. Eng. B57, 179-185 (1999).
9. J.M.S. Skakle, Mat. Sci. Eng. R23, 1-40 (1998).
10. M. Murakami, S.I. Yoo, T. Higuchi, N. Sakai, J. Weltz, N. Koshizuka, and S. Tanaka, Jpn. J. Appl. Phys. 33, L715 (1994).
11. F. Prado, A. Caneiro, and A. Sequis, Physica C 295, 235-246 (1998).
12. M. Boffa, A Di Trolio, S. Pace, A. Saggese and A. Vecchione, IEEE Trans. Appl. Supercond. 7, 2 (1997).
13. M. Muralidhar and M. Murakami, Appl. Supercond. 5, 1-6, 127-131 (1997).
14. J.R. Olive, Ph.D. Dissertation, Vanderbilt University (1998).
15. J.R. Olive, W.H. Hofmeister, R.J. Bayuzick, and M. Vlasse, J. Mater. Res. 14, 10, 3851-58 (1999).
16. J.K.R. Weber, D.S. Hampton, D.R. Merkley, C.A. Rey, M.M. Zatarski, and P.C. Nordine, Ceram. Bull. 70, 1, 71 (1991).
17. F. Prado, A. Caneiro, and A. Sequis, Physica C 295, 235-246 (1998).
18. M. Kambara, M. Nakamura, Y. Shiohara, and T. Umeda, Physica C 275, 127-134 (1997).
19. J.R. Olive, W.H. Hofmeister, R.J. Bayuzick, and M. Vlasse, J. Mater. Res. 14, 10, 3851-58 (1999).
20. M. Kambara, T. Umeda, M. Tagami, X. Yao, E.A. Goodilin, and Y. Shiohara, J. Am. Ceram. Soc. 81 [8] 2116 (1998).
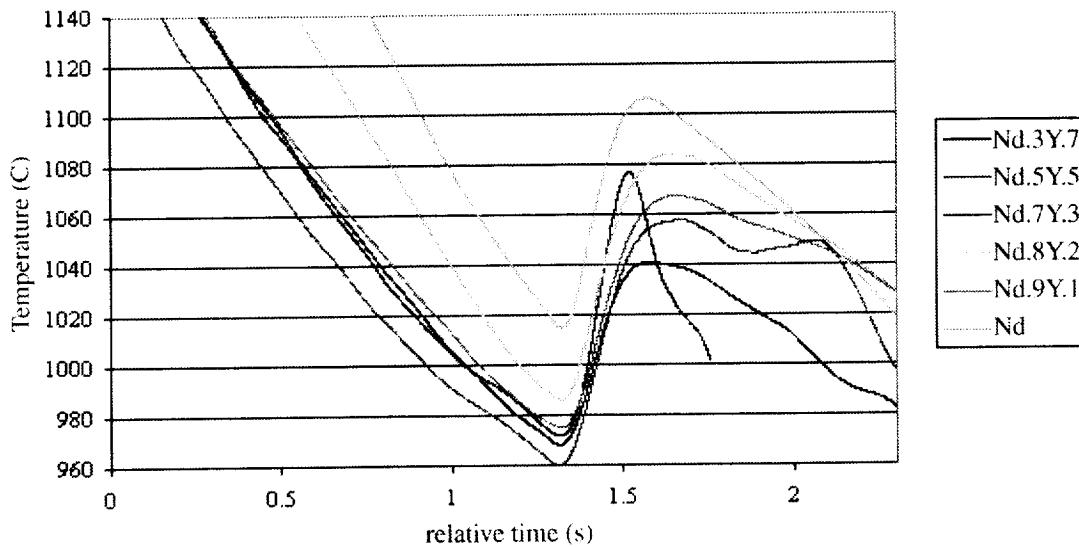
Figure 1. A compilation of pyrometry data for Y/Nd123 alloy samples. The curves were obtained by determining the average trace of several recalescence events for each composition, synchronizing the time-temperature plots at the moment of recalescence, and adjusting the temperature by the *in-situ* calibration factor.
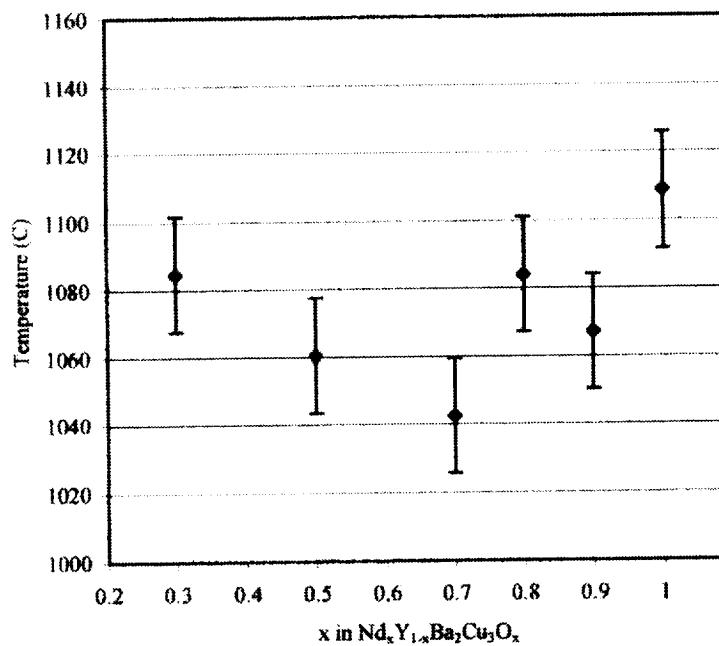
Figure 2. Experimentally determined average peritectic temperatures for Nd/Y123 binary alloy samples processed in the AAL. The temperature has been corrected using Nd123 as an *in-situ* calibration. The standard deviation in the data was used to calculate the magnitude of the error bars.

306
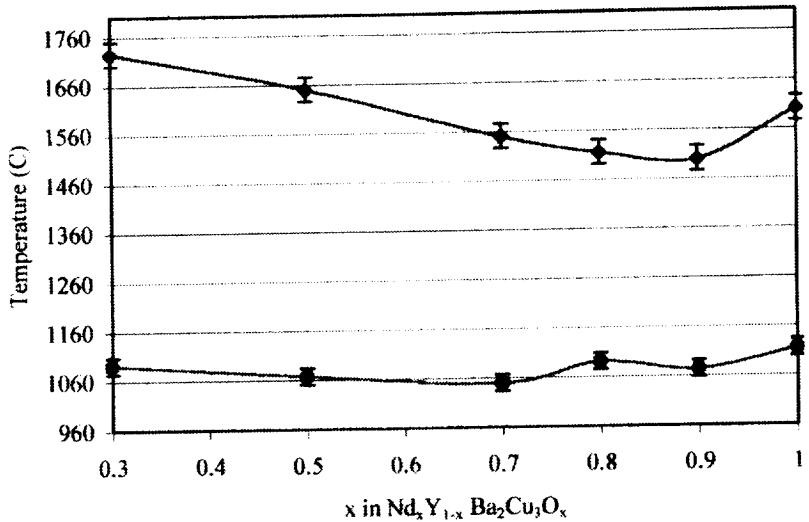
Figure 3. Trace of the Nd/Y123 liquidus and peritectic in pure O_2. Liquidus temperatures were obtained from drop tube work performed by Olive and peritectic temperatures represent corrected experimental data from this work.
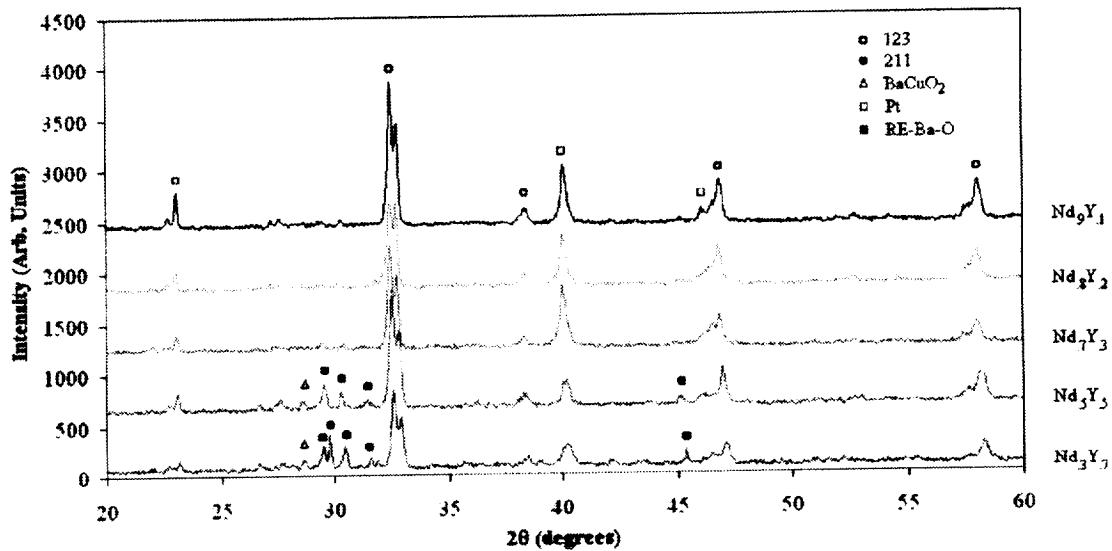
Figure 4. A compilation of XRD spectra for Y/Nd123 alloys processed in the AAL. RE123 is the dominant phase for all compositions. The appearance of RE211 in the scans becomes more prevalent in Y-rich compounds.